



ISSN: 1813-162X (Print); 2312-7589 (Online)

Tikrit Journal of Engineering Sciences

available online at: <http://www.tj-es.com>
TJES
 Tikrit Journal of
 Engineering Sciences

Direct Torque Control Space Vector Modulation for Induction Motor Driven by Matrix Converter

 Ayad T. Mahmood ^{a*}, Khalaf S. Gaeid ^a, Takiaddin A. Al Smadi ^b
^a Department of Electrical Engineering, College of Engineering, Tikrit University, Tikrit, Iraq.^b Faculty of Engineering, Jerash University, Jerash, Jordan.

Keywords:

Matrix Converter (MC); Space vector pulse width modulation (SVPWM); Space vector modulation (SVM); Direct torque control (DTC); Induction motor (IM).

Highlights:

- Impact of different interior extended surface area of digesters on AD performance.
- CD was used as a substrate in digesters under mesophilic conditions.
- Digester D has a favored performance due to high extended surface area.

ARTICLE INFO

Article history:

Received	02 Feb.	2024
Received in revised form	08 Apr.	2024
Accepted	18 Apr.	2024
Final Proofreading	05 Sep.	2024
Available online	15 Oct.	2024

© THIS IS AN OPEN ACCESS ARTICLE UNDER THE CC BY LICENSE. <http://creativecommons.org/licenses/by/4.0/>



Citation: Mahmood AT, Gaeid KS, Al Smadi TA. Direct Torque Control Space Vector Modulation for Induction Motor Driven by Matrix Converter.

Tikrit Journal of Engineering Sciences 2024; 31(4): 58-69.

<http://doi.org/10.25130/tjes.31.4.6>

*Corresponding author:

Ayad T. Mahmood

Department of Electrical Engineering, College of Engineering, Tikrit University, Tikrit, Iraq.



Abstract: This study proposes enhancing induction motor (IM) drive systems by developing a DTC-MC with SVPWM integration to reduce ripple. DTC-MC is effective for precise torque control in AC drives, offering high control accuracy by isolating stator flux and torque. The method excels in sensor-less speed control, maintaining unity input power factor at low speeds, and constant switching frequency for rapid torque adjustments. Combining DTC-MC with SVPWM improves simplicity, dynamic behavior, and torque response. The DTC-SVM approach further refines the torque response by correcting flux and torque discrepancies. MATLAB/SIMULINK simulations validated the approach, showing a robust dynamic response and significantly reduced motor torque ripple and control of speed.

السيطرة على المحركات الحثية عن طريق محول المصفوفة باستخدام تعديل ناقل الفضاء للتحكم المباشر في عزم الدوران

اياد طارق محمود¹، خلف سلوم كعبيد¹، تقى الدين الصمادي²

¹ قسم الهندسة الكهربائية/ كلية الهندسة/ جامعة تكريت/ تكريت - العراق.

² كلية الهندسة/ جامعة جرش/ جرش - الأردن.

الخلاصة

تقترح هذه الدراسة تعزيز أنظمة المحركات الحثية من خلال تطوير نظام DTC-MC مع تقنية SVPWM لتقليل التمرج. يعتبر DTC-MC فعالاً للتحكم الدقيق في عزم الدوران في محركات التيار المتردد، مما يوفر دقة تحكم عالية عن طريق عزل تدفق الجزء الثابت وعزم الدوران. تتفوق هذه الطريقة في التحكم في السرعة بدون مستشعر، والحفاظ على عامل طاقة الإدخال الموحد عند السرعات المنخفضة، وتردد التبديل الثابت لإجراء تعديلات سريعة على عزم الدوران. يعمل الجمع بين DTC-MC و SVPWM على تحسين البساطة والسلوك الديناميكي واستجابة عزم الدوران. يعمل نهج DTC-SVM على تحسين ذلك عن طريق تصحيح تباينات التدفق وعزم الدوران. أثبتت عمليات محاكاة MATLAB/SIMULINK صحة هذا النهج، وأظهرت استجابة ديناميكية قوية وتقليل تمرج عزم دوران المحرك بشكل كبير والتحكم في السرعة. **الكلمات الدالة:** محول المصفوفة (MC)، تعديل عرض نبض ناقل الفضاء (SVPWM)، تعديل ناقل الفضاء (SVM)، التحكم المباشر في عزم الدوران (DTC)، المحرك الحثي (IM).

1. INTRODUCTION

In the last two decades, the need for improved power supply quality and efficiency has catapulted the three-phase matrix converter into a prominent position as a contemporary energy converter, which has risen as a superior choice to traditional energy conversion modules. Matrix converter-driven motor systems surpass PWM inverter drives due to their capacity for two-way power transfer, generation of sine-shaped input and outcome currents, and the flexibility to adjust the power factor at the input. Moreover, MCs facilitate small and efficiently organized designs by eliminating the necessity for components storing energy, such as capacitors in the DC-link. Nevertheless, the practical application of matrix converters in vector control systems for (IM) has been constrained because the modulation techniques and switching control require a higher quantity of intricate than those employed in conventional PWM power inverters [1]. Since the mid-1980s, the Direct Control (DTC) approach has become widely accepted in variable-speed drive applications, especially when achieving precise control over torque is prioritized over speed regulation. Typically, IMs can be controlled using two methods, known as scalar and vector control (VC), which can be implemented as open or closed-loop systems. Vector control focuses on regulating the rotor flux and torque by estimating the motor by speed and voltage, which can be determined directly or indirectly. An uncomplicated substitute for vector control is the DTC [2]. DTC has several notable benefits, including quick transient torque response and low computational demands. Nonetheless, traditional DTC has two distinct drawbacks: variable switching frequencies that rely on hysteresis bands and motor speed, and it produces significant torque fluctuations, especially compared to the Field-Oriented Control method. To mitigate torque fluctuations in traditional DTC, the typical approach involves reducing the sampling

interval, which results in higher switching frequencies [3]. Various endeavors have enhanced the stable-state capabilities of DTC techniques, including adopting Direct Self Control (DSC), utilizing SVM, incorporating multilevel inverters, integrating with Matrix Converters, and implementing Predictive Torque Control. When the strengths of MCs are merged with those of DTC methods, it becomes feasible to attain swift torque and flux responses over a broad speed range [4], as explained in the following studies and research [5]. This article introduces a DTC scheme using SVPWM for a five-phase IM powered by a 3×5 phase DMC. It focuses on eliminating the third harmonic in the xy plane via SVPWM-VV and volt-second balancing. SVPWM-VVs impact stator flux, torque, speed, and power factor, reducing torque and stator current ripple while maintaining a consistent switching frequency. It also employs a LUT to regulate input power factor and grid current harmonics at [6]. As a validation of the work presented in this paper, the same results were obtained as shown in [7, 8]. They developed a direct torque-controlled matrix converter-fed induction motor drive system based on the space vector modulation technique (SVPWM) for ripple reduction. DTC-MC combination is an efficient way to get better performance specifications in the industry. The direct torque control technique is used in AC drive systems to obtain high-performance torque control. The DTC-SVM combination method on the matrix converter has been successfully used for the IM to reduce torque ripples. Since torque control and ripple reduction were the main goals, the DTC-SVM technique minimizes the torque and flux error. Constant switching frequency DTC-SVM schemes considerably improved the drive performance in reduced torque and flux pulsations and low-speed operation, well-defined radiated noise, and a harmonic spectrum. The contribution of the present work can be explained as follows: controlling the

matrix converter using DTC-SVM technology, controlling the speed of the IM, and reducing distortions in voltage and current using the appropriate filter. The present work is organized as follows: section 1 studies the DTC structure, section 2 explains the concept of space vectors, section 3 explains the DTC Matrix Converter structure, section 4 shows clear LC input filters, and section 5 shows the simulation and result.

2. DTC STRUCTURE

The fundamental framework of the DTC-IM system is depicted in Fig. 1. The underlying fundamental concept of the DTC method can be explained as outlined below: Initially, the system measures phase currents and voltages. These measurements are sent for the flux and torque estimation module, which calculates the natural system flux and torque values. The computed torque is subsequently contrasted to its reference values in the torque controller, while the actual flux is contrasted against the reference flux values in the controller. The control signal for the IGBTs is generated using the outputs from the stator flux and torque controllers, serving as inputs for the DTC switching look-up table [9]. This paper presents an enhanced DTC approach where the reference stator voltage vectors were generated based on torque and flux errors, as indicated in Eqs. (1) to (5) below. These reference stator voltage vectors are then modulated using the SVPWM technique [10, 11]. The component related to the field is oriented along the d-axis, while the torque component is allocated synchronized with the q-axis, and both components are mutually perpendicular to one another. Stator voltage given in Eq. (1) and rotor voltage given in Eq. (2):

$$v_s = R_s i_s + \frac{d\gamma_s}{dt} \quad (1)$$

$$v_r = R_r i_r + \frac{d\gamma_r}{dt} - j\omega_m \gamma_r \quad (2)$$

The variables λ_s and λ_r represent the flux linkage of the stator and rotor, measured in Weber (Wb). The variables i_s and i_r represent the current flowing through the stator and rotor, measured in Amperes (A). Similarly, R_s and R_r denote the resistance of the stator and rotor, measured in Ohms (Ω), respectively. The equation for stator flux and flux in the rotor are as follows:

$$\lambda_s = L_m i_r + L_s i_s \quad (3)$$

$$\lambda_r = L_m i_s + L_r i_r \quad (4)$$

where Mutual inductance is denoted in Henrys as L_m , and L_s and L_r represent the stator and rotor inductances, respectively, also measured in Henrys [12]. The torque developed by the motor given from Eq. (5) [13, 14]:

$$T = \frac{3p}{2} (\gamma_{ds} i_{qs} - \gamma_{qs} i_{ds}) \quad (5)$$

The variables i_{qs} and i_{ds} represent the stator flux linkages in Weber for the q-axis and d-axis, and λ_{qr} and λ_{ds} represent the rotor flux linkages in Weber for the q-axis and d-axis, respectively. The inverter's switch settings are determined by the disparities in torque and flux, which are determined by sector identification, ensuring the estimated stator flux and torque stay within their predetermined thresholds, as shown in Fig. 2. During every sampling interval, estimations for torque and stator flux are made and subsequently assessed by the hysteresis comparator against their corresponding reference values [15].

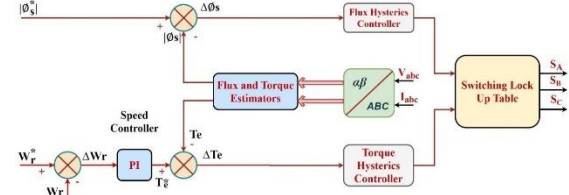


Fig. 1 Block Diagram of DTC.

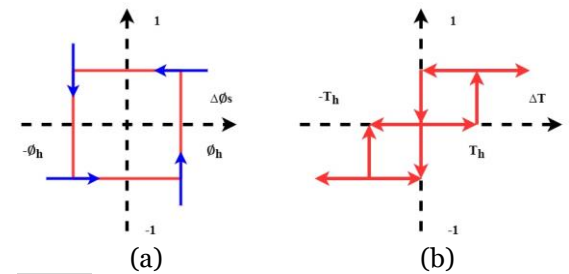


Fig. 2 (a) Flux Hysteresis Comparison Module (b) Torque Hysteresis Comparison Module.

3. THE CONCEPT OF SPACE VECTORS

The idea of space vectors, originating in the rotating domain of IMs, finds application in the modulation of inverter output voltage. In this technique, the three-phase values are converted into their respective two-phase equivalents, either in a frame that rotates in synchrony or a stationary frame. The magnitude of the reference vector is expressed through these dual-phase constituents. Moreover, it is subsequently employed to modulate the inverter's output. The procedure for acquiring the revolving spatial vector is elaborated in the next section, focusing on the fixed reference frame. Within the fixed reference frame, the trinary sinusoidal voltage element is assumed as [16]:

$$V_a = V_m \sin \omega t \quad (6)$$

$$V_b = V_m \sin \left(\omega t - \frac{2\pi}{3} \right) \quad (7)$$

$$V_c = V_m \sin \left(\omega t - \frac{4\pi}{3} \right) \quad (8)$$

When three-phase voltage is supplied to the AC machine, it creates a rotating magnetic field in the machine's air gap. This rotating magnetic field can be expressed as a sole rotating voltage vector. Clark's Transformation is employed to determine the magnitude and direction of this rotating vector within the stationary reference

frame. For implementing SVPWM, the voltage equations in the *abc* reference frame are converted into the stationary dq reference frame, comprising the horizontal (d) and vertical (q) axes [17], as depicted in Fig. 3, illustrating the connection between these two reference frames in Eqs. (9) and (10).

$$l_{dq0} = M_s * l_{abc} \tag{9}$$

$$M_s = \frac{2}{3} * \begin{bmatrix} 1 & -1/2 & -1/2 \\ 0 & -\sqrt{3}/2 & \sqrt{3}/2 \\ 1/2 & 1/2 & 1/2 \end{bmatrix}, l_{dq0} =$$

$$[l_d l_q l_0]^T, l_{abc} = [l_a l_b l_c]^T \tag{10}$$

Where *l* represents an electrical variable, which could be either a voltage or a current.

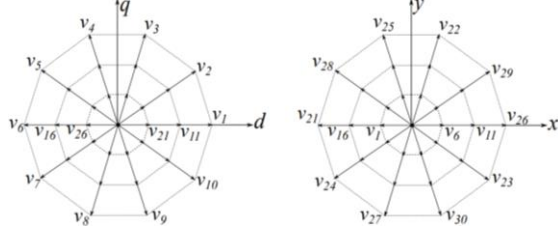


Fig. 3 SVPWM for dq and xy Axes [18].

The Park's conversion process involves transforming $\alpha\beta$ to dq coordinates, simultaneously rotating α and β axes utilizing a predefined frequency. This reference frequency is conveyed via the input related to the phase (ωt), as illustrated in Fig. 4 [19].

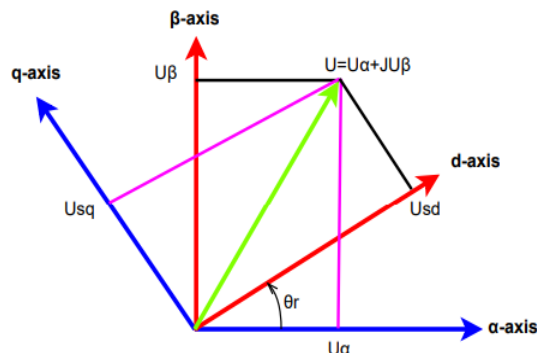


Fig. 4 Conversion of Coordinates from the α - β Frame to the d-q Frame $U_\alpha U_\beta$.

In Fig. 3, this transformation essentially projects [a b c]^t orthogonally onto a two-dimensional plane orthogonal to the vector [1 1 1]^t, forming what is known as the d-q plane within a spatial three-dimensional coordinate system. This transformation allows for the existence of six nonzero vectors (V1 through V6), which establish the vertices of a hexagonal shape, as shown in Fig. 5, and are responsible for supplying power delivered to the load. The angle between each consecutive pair of these nonzero vectors is 60 degrees. Additionally, two zero vectors (V0 and V7) are at the origin, with zero voltage applied to the load. These eight vectors are collectively referred to as the basic space vectors (V0, V1, V2, V3, V4, V5, V6, and V7). A similar transformation is employed to

obtain the desired reference voltage vector, *Vref*, within the d-q plane from the desired output voltage. The primary objective of the SVPWM technique is to approximate *Vref* by utilizing the eight switching patterns. A straightforward approach to achieving this aim is to approximately ensure that the average inverter output within a short time T matches *Vref* within an identical time frame [20].

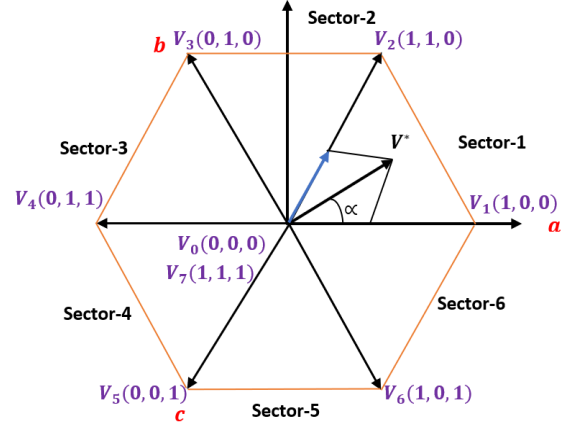


Fig. 5 SVPWM Sectors and Switching Vectors Representation.

For the operation mode spanning 180 degrees, there are six distinct switching states and a pair of additional states where either entirely upper or entirely lower arm switches are turned on. These eight states can be represented with three bits in binary form ($2^3 = 8$). As upper and lower switches consistently operate complementary, it is sufficient to indicate the upper bridge switch status. In this representation, "1" indicates the switch is on, and "0" indicates it is off. Table 1 tabulates detailed information on these eight states' phase and line voltages [21].

Table 1 Visualizes Voltage Space Vector Switching Patterns About Phase and Line Voltages.

Vector	Switching vector	The line to neutral voltage			Line-to-line voltage		
	$s_1 s_2 s_3$	V_{an}	V_{bn}	V_{cn}	V_{ab}	V_{bc}	V_{ca}
V0	000	0	0	0	0	0	0
V1	100	$\frac{2}{3}V_{dc}$	$-\frac{1}{3}V_{dc}$	$-\frac{1}{3}V_{dc}$	V_{dc}	0	$-V_{dc}$
V2	110	$\frac{1}{3}V_{dc}$	$\frac{1}{3}V_{dc}$	$-\frac{2}{3}V_{dc}$	0	V_{dc}	$-V_{dc}$
V3	010	$-\frac{1}{3}V_{dc}$	$\frac{2}{3}V_{dc}$	$-\frac{1}{3}V_{dc}$	$-V_{dc}$	V_{dc}	0
V4	011	$-\frac{2}{3}V_{dc}$	$\frac{1}{3}V_{dc}$	$\frac{1}{3}V_{dc}$	$-V_{dc}$	0	V_{dc}
V5	001	$-\frac{1}{3}V_{dc}$	$-\frac{1}{3}V_{dc}$	$\frac{2}{3}V_{dc}$	0	$-V_{dc}$	V_{dc}
V6	101	$\frac{1}{3}V_{dc}$	$-\frac{2}{3}V_{dc}$	$\frac{1}{3}V_{dc}$	V_{dc}	$-V_{dc}$	0
V7	111	0	0	0	0	0	0

4.DTC MATRIX CONVERTER STRUCTURES

The various topologies of multiphase converters can be categorized as shown in Fig.6 [22]. On one hand, these configurations can be categorized according to the power conversion method, either as AC-DC-AC or AC-AC modes. AC-AC converters are called MCs and consist of direct and indirect types. Conversely, considering the neutral point connections,

multiphase configurations can be categorized as open-winding or single-sided modes. In open-winding configurations, which lack a neutral point connection, both ends can receive power from either a single or two separate DC sources. Furthermore, single-ended topologies might feature one or multiple central point's [23].

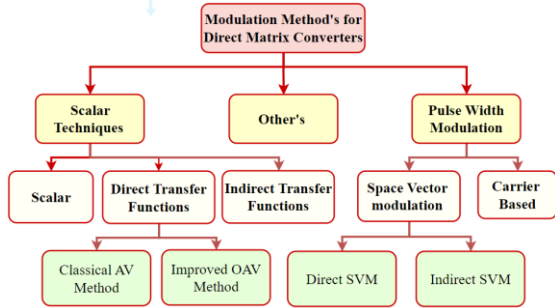


Fig. 6 Categorization of Multiphase Converter Configurations.

The matrix converter utilizes a configuration of 9 switches that can be operated in both directions, enabling the connection from any output phase to any input phase. The converter's input terminals are linked to a voltage-fed system comprising three phases, typically sourced from the grid. On the other hand, the output connections are connected to a system where current is supplied consisting of three phases, similar to what was employed in an IM [24]. The MC employs a one-stage conversion unit that utilizes bidirectional switches instead of multiple conversion stages and energy storage components commonly found in conventional converters [25]. Figure 7 presents a simplified block diagram of the matrix converter, known for its compact and capacitor-free design. This configuration offers 27 switching states, allowing 27 potential space vectors to control the IM. These states are grouped into three categories: Group I connected one input line to two output lines, Group II linked all output lines to a common input line, and Group III established connections between each output line and a distinct input line.

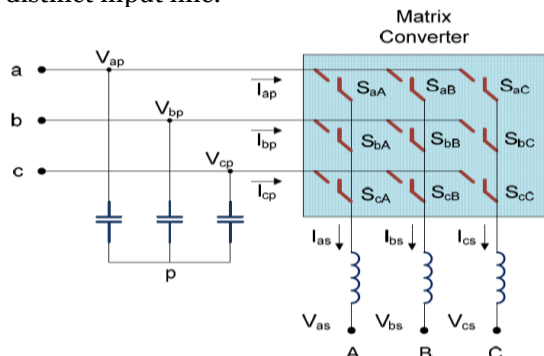


Fig. 7 Matrix Converts Schematic Diagram [6].

The matrix converter offers a total of 27 different switching configurations. These

configurations are detailed in Table 2, where their associated output voltage and input current vectors can be found. These switching arrangements can be categorized into three primary groups:

- 1- Zero vectors labeled as 0_a to 0_c , which have no magnitude.
- 2- Rotating vectors with a consistent magnitude but changeable direction ranging from ± 10 to ± 12 .
- 3- Active vectors with a fixed direction but adjustable magnitude spanning from ± 1 to ± 9 [26].

Table 2 Eight Hexagon States, each Associated with Specific Phase Voltages and Space.

State	Mode	On Switches	v_o	α_o	i_i	β_i
0_a	AAA	$S_{Aa} S_{Ab} S_{Ac}$	0	-	0	-
0_b	BBB	$S_{Ba} S_{Bb} S_{Bc}$	0	-	0	-
0_c	CCC	$S_{Ca} S_{Cb} S_{Cc}$	0	-	0	-
+10	ABC	$S_{Aa} S_{Bb} S_{Cc}$	v_{imax}	α_i	i_{omax}	β_o
-10	ACB	$S_{Aa} S_{Cb} S_{Bc}$	v_{imax}	$-\alpha_i$	i_{omax}	$-\beta_o$
+11	CAB	$S_{Ca} S_{Ab} S_{Bc}$	v_{imax}	$\alpha_i + \frac{2\pi}{3}$	i_{omax}	$\beta_o + \frac{2\pi}{3}$
-11	BAC	$S_{Ba} S_{Ab} S_{Cc}$	v_{imax}	$-\alpha_i + \frac{2\pi}{3}$	i_{omax}	$-\beta_o + \frac{2\pi}{3}$
+12	BCA	$S_{Ba} S_{Cb} S_{Ac}$	v_{imax}	$\alpha_i + \frac{4\pi}{3}$	i_{omax}	$\beta_o + \frac{4\pi}{3}$
-12	CBA	$S_{Ca} S_{Bb} S_{Ac}$	v_{imax}	$-\alpha_i + \frac{4\pi}{3}$	i_{omax}	$-\beta_o + \frac{4\pi}{3}$
+1	ABB	$S_{Aa} S_{Bb} S_{Bc}$	$\frac{2}{3}v_{AB}$	0	$\frac{2}{\sqrt{3}}i_a$	$\frac{\pi}{6}$
-1	BAA	$S_{Ba} S_{Ab} S_{Ac}$	$\frac{-2}{3}v_{AB}$	0	$\frac{-2}{\sqrt{3}}i_a$	$\frac{-\pi}{6}$
+2	BCC	$S_{Ba} S_{Cb} S_{Cc}$	$\frac{2}{3}v_{BC}$	0	$\frac{2}{\sqrt{3}}i_b$	$\frac{\pi}{2}$
-2	CBB	$S_{Ca} S_{Bb} S_{Bc}$	$\frac{-2}{3}v_{BC}$	0	$\frac{-2}{\sqrt{3}}i_b$	$\frac{\pi}{2}$
+3	CAA	$S_{Ca} S_{Ab} S_{Ac}$	$\frac{2}{3}v_{CA}$	0	$\frac{2}{\sqrt{3}}i_a$	$\frac{7\pi}{6}$
-3	ACC	$S_{Aa} S_{Cb} S_{Cc}$	$\frac{-2}{3}v_{CA}$	0	$\frac{-2}{\sqrt{3}}i_a$	$\frac{7\pi}{6}$
+4	BAB	$S_{Ba} S_{Ab} S_{Bc}$	$\frac{2}{3}v_{AB}$	$\frac{2\pi}{3}$	$\frac{2}{\sqrt{3}}i_b$	$\frac{-\pi}{6}$
-4	ABA	$S_{Aa} S_{Bb} S_{Ac}$	$\frac{-2}{3}v_{AB}$	$\frac{2\pi}{3}$	$\frac{-2}{\sqrt{3}}i_b$	$\frac{-\pi}{6}$
+5	CBC	$S_{Ca} S_{Bb} S_{Cc}$	$\frac{2}{3}v_{BC}$	$\frac{2\pi}{3}$	$\frac{2}{\sqrt{3}}i_b$	$\frac{\pi}{2}$
-5	BCB	$S_{Ba} S_{Cb} S_{Bc}$	$\frac{-2}{3}v_{BC}$	$\frac{2\pi}{3}$	$\frac{-2}{\sqrt{3}}i_b$	$\frac{\pi}{2}$
+6	ACA	$S_{Aa} S_{Cb} S_{Ca}$	$\frac{2}{3}v_{CA}$	$\frac{2\pi}{3}$	$\frac{2}{\sqrt{3}}i_b$	$\frac{7\pi}{6}$
-6	CAC	$S_{Ca} S_{Ab} S_{Cc}$	$\frac{-2}{3}v_{CA}$	$\frac{2\pi}{3}$	$\frac{-2}{\sqrt{3}}i_b$	$\frac{7\pi}{6}$
+7	BBA	$S_{Ba} S_{Bb} S_{Ac}$	$\frac{2}{3}v_{AB}$	$\frac{4\pi}{3}$	$\frac{2}{\sqrt{3}}i_c$	$\frac{-\pi}{6}$
-7	AAB	$S_{Aa} S_{Ab} S_{Bc}$	$\frac{-2}{3}v_{AB}$	$\frac{4\pi}{3}$	$\frac{-2}{\sqrt{3}}i_c$	$\frac{-\pi}{6}$
+8	CCB	$S_{Ca} S_{Cb} S_{Bc}$	$\frac{2}{3}v_{BC}$	$\frac{4\pi}{3}$	$\frac{2}{\sqrt{3}}i_c$	$\frac{\pi}{2}$
-8	BBC	$S_{Ba} S_{Bb} S_{Cc}$	$\frac{-2}{3}v_{BC}$	$\frac{4\pi}{3}$	$\frac{-2}{\sqrt{3}}i_c$	$\frac{\pi}{2}$
+9	AAC	$S_{Aa} S_{Ab} S_{Cc}$	$\frac{2}{3}v_{CA}$	$\frac{4\pi}{3}$	$\frac{2}{\sqrt{3}}i_c$	$\frac{7\pi}{6}$
-9	CCA	$S_{Ca} S_{Cb} S_{Ac}$	$\frac{-2}{3}v_{CA}$	$\frac{4\pi}{3}$	$\frac{-2}{\sqrt{3}}i_c$	$\frac{7\pi}{6}$

Consequently, Table 3 elucidates the relationship between the DTC method's voltage vectors and switching states across different voltage sectors [27].

Table 3 Matrix Converter Switching.

Voltage vector	Voltage sector					
	1	2	3	4	5	6
\vec{V}_1	-3, +1	+2, -3	-1, +2	+3, -1	-2, +3	+1, -2
\vec{V}_2	+9, -7	-8, +9	+7, -8	-9, +7	+8, -9	-7, +8
\vec{V}_3	-6, +4	+5, -6	-4, +5	+6, -4	-5, +6	+4, -5
\vec{V}_4	+3, -1	-2, +3	+1, -2	-3, +1	+2, -3	-1, +2
\vec{V}_5	-9, +7	+8, -9	-7, +8	+9, -7	-8, +9	+7, -8
\vec{V}_6	+6, -4	-5, +6	+4, -5	-6, +4	+5, -6	-4, +5

Figure 8 illustrates the block diagram of DTC-MC-SVM. To provide a concise overview of the fundamental DTC principles when employing MCs, it can be summarized as follows: During each sampling interval, the appropriate switching arrangement is chosen. This selection enables the correction of immediate deviations in stator flux magnitude and torque while adhering to the unity input power factor constraint [14] and feeding the IM [28]. The DTC (Direct Torque Control) employs a general selection table represented by the sector number "M" detailed in Table 4. In DTC, the null sequence vectors (V000 or V111) sustain rotational force consistency and are inactive within the switching duration. The DTC switching table enables selecting vector positions to apply to the Motor Controller based on the direct component (DC) of stator flux and electromagnetic torque, as demonstrated in Table 5. Observing Table 4, it becomes evident that the switching frequency of IGBTs. (Insulated Gate Bipolar Transistors) utilized in this approach is variable. Controlling the permissible ranges makes maintaining the average switching frequency at reference possible, thereby minimizing ripple current and torque fluctuations [29].

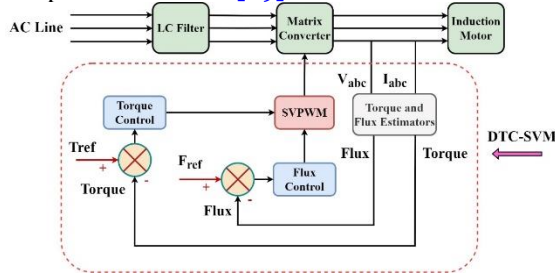


Fig. 8 Diagram Illustrating the Operation of DTC-MC-SVM.

Table 4 Table for General Selection.

Ψ_s in sector M	Torque	
	Increase	Decrease
Flux	Increase Decrease	V_{m+1} V_{m+2} V_{000} V_{111}

Table 5 DTC-MC Switching Table.

		Sector					
		1	2	3	4	5	6
$d\phi = +1$	$dT = 0$	V_0	V_7	V_0	V_7	V_0	V_7
	$dT = +1$	V_2	V_3	V_4	V_5	V_6	V_1
	$dT = -1$	V_6	V_1	V_2	V_3	V_4	V_5
$d\phi = -1$	$dT = 0$	V_7	V_0	V_7	V_0	V_7	V_0
	$dT = +1$	V_3	V_4	V_5	V_6	V_1	V_2
	$dT = -1$	V_5	V_6	V_1	V_2	V_3	V_4

5. LC INPUT FILTERS

An analytical approach assessed the optimized parameters' performance quality and defined optimization constraints. The parameters of LC filters are interrelated through the cut-off frequency formula, also known as the resonance frequency given in Eq. (11).

$$f_{cut} = \frac{1}{2\pi\sqrt{LC}} \quad (11)$$

From the formula above, it can be inferred that two of the three variables, namely f_{cut} , L, and C, must be chosen arbitrarily. In systems

employing a constant switching period, such as those utilizing Pulse Width Modulation, the cut-off frequency is typically set slightly below the switching frequency. However, the DTC algorithm operates with a variable switching period, making the precise determination of its value challenging. It is important to note that the inductance value significantly influences the size and cost of a coil. Considering these factors, it is most advantageous to treat the inductance and cut-off frequency of the filter as arbitrarily chosen parameters. To calculate the third parameter, capacity, using transform the formula given in Eq. (12):

$$C = \frac{1}{4\pi^2 f_{cut}^2 L} \quad (12)$$

This kind of filter is responsible for the suppression of high current and voltage harmonics introduced by the converter. Without it, the MC cannot function stable [30, 31]. The transfer function $H(s)$ for the continuous-time input signal and output of the filter given in Eq. (13), then the cut-off frequency ($f_c=355.88$ Hz), Quality factor = 2.236, Damping ratio = 4.45, and poles = 355.88 Hz.

$$H(s) = \frac{1/LC}{s^2 + \frac{R}{L}s + 1/LC} \quad (13)$$

6. SIMULATION MODEL AND RESULTS

In this study, the induction motor was controlled using a matrix converter consisting of 18 IGBTs, through which the SVM-DTC technology was used, which is considered one of the most influential and fast techniques for solving problems. Thus, the signals of all IGBTs are suppressed, ensuring no interference between the electrical signals. An appropriate input filter was used to guarantee that the current and voltage signals entering the matrix converters were undistorted. Thus, the power factor will be unity, as shown in the present study. The speed was precisely controlled, and the response of the induction motor to all variables was swift due to using the SVM-DTC technology. To evaluate the effectiveness of the suggested method, simulations were conducted using a sampling interval of 20 microseconds. The closed-loop model used for system simulation is depicted in Fig. 9. The simulation employed a 4-kW squirrel-cage induction motor with three phases as the machine model: $P_i=2.5$ kW, $V_n=480$ V, $R_s=0.6$ Ω , $R_r=0.65$ Ω , $L_s=1.8$ mH, $L_r=1.8$ mH, $L_m=65.33$ mH, $J=0.05$ kg.m², and $P=2$. The best parameters analytical and optimized of input filters were $L=1$ mH and $C=200$ μ f. Figure 10 illustrates the input voltages and currents of phase-a during steady-state operation. The currents exhibited sinusoidal characteristics and maintained phase alignment with the voltages, indicating a unity power factor using the appropriate LC input filter. Figure 11 displays the desired speed setting and the corresponding speed tracking,

which align perfectly as the speed command transitions from 500 RPM to 700 RPM and decreases back to 500 RPM and 0 RPM. During the initial phase of the loading process, noteworthy events concerning torque, particularly the torsional force, occurred. Initially, the electrically generated torque began at zero and gradually increased to +15 Nm, as depicted in Fig. 12. This initial response provides insight into the system's reaction to varying torque loads, ultimately finding equilibrium. Therefore, it follows the torque reference to the induction motor. Figure 13 shows the stator current signal in the simulated time domain. The stator current peaked at about 28 A during startup, and the rotor speed decreased the moment the plate entered operation; however, the speed was controlled according to the input speed reference. Figures 14 and 15 illustrates the pulses generated by dtc- svm techniques to control of MC and also achieve that is no interference signals. Figure 16 illustrates that the adaptive observer can estimate the stator flux well and truly. The

stator voltage for the dq axes, as shown in Fig.17, refers to the voltage components in the dq-axis coordinate system. These voltage components are typically expressed as V_d and V_q , representing the voltage in the direct (d) and quadrature (q) axes, respectively. In Fig. 18, the Flux rotor for dq axes illustrates the concept used to analyze and control the magnetic field produced by the rotor of an electric machine within the context of the dq reference frame, making designing, controlling, and optimizing electric drives and synchronous machines easier. Different parameters and speed references of the induction motor were applied, illustrated in Fig.19. The bode gain and phase plots provide a direct and accurate method to depict gain and phase-shift properties in circuit and control theory. They are valuable tools for frequency domain analysis, allowing a practical examination of these aspects through experimental representation, as illustrated in Fig. 20.

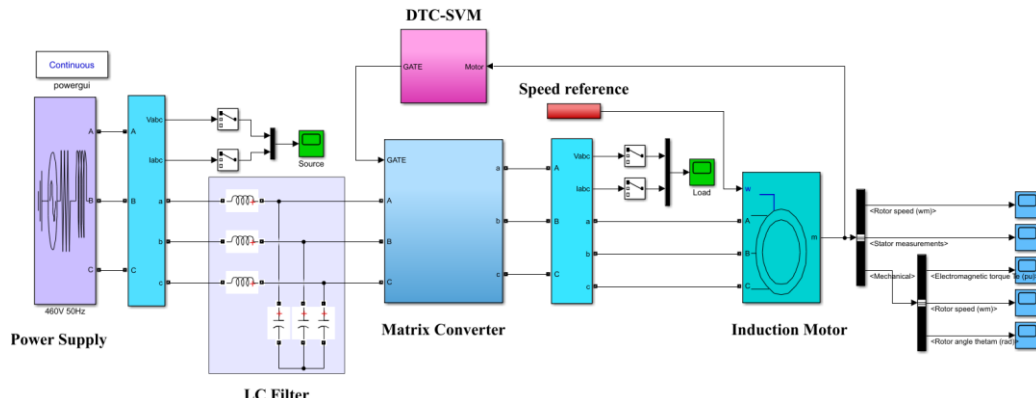


Fig. 9 The Simulation Model for (MC-DTC-IM).

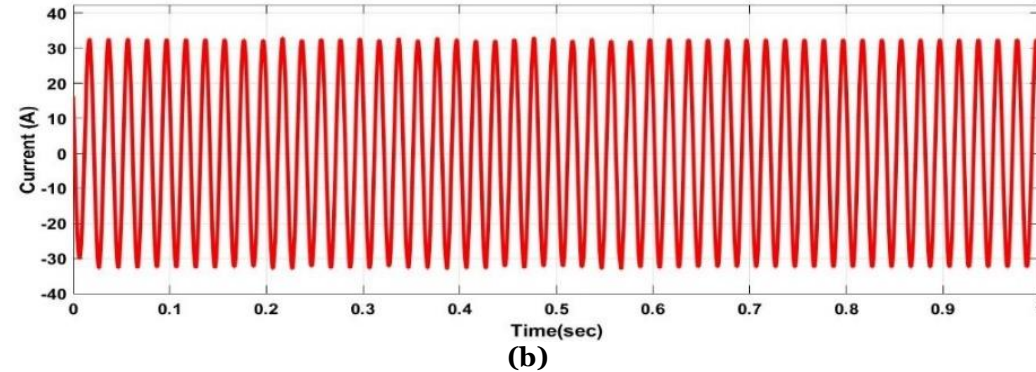
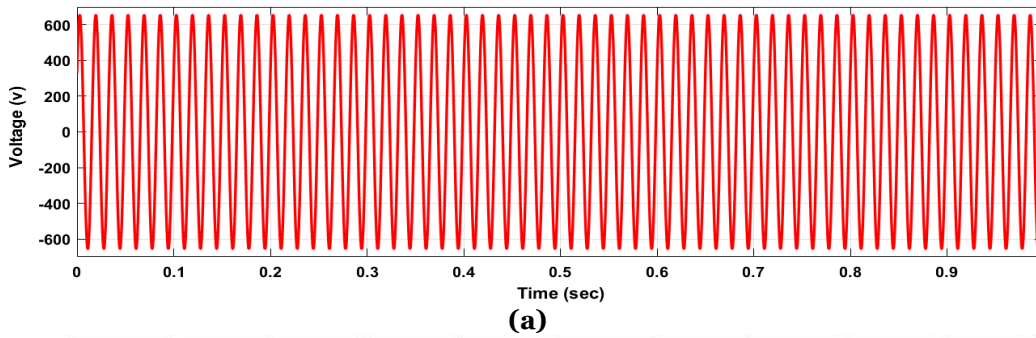


Fig. 10 Input Voltage and Current of MC (a) Input Voltage of Phase a (b) Input Current of Phase a.

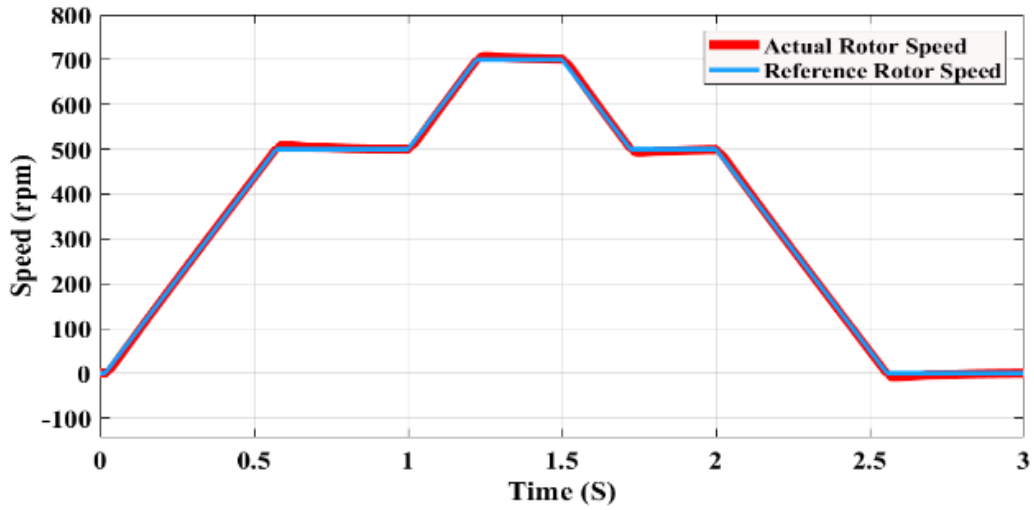


Fig. 11 Speed Reference in (blue) and Actual Speed Response in (Red).

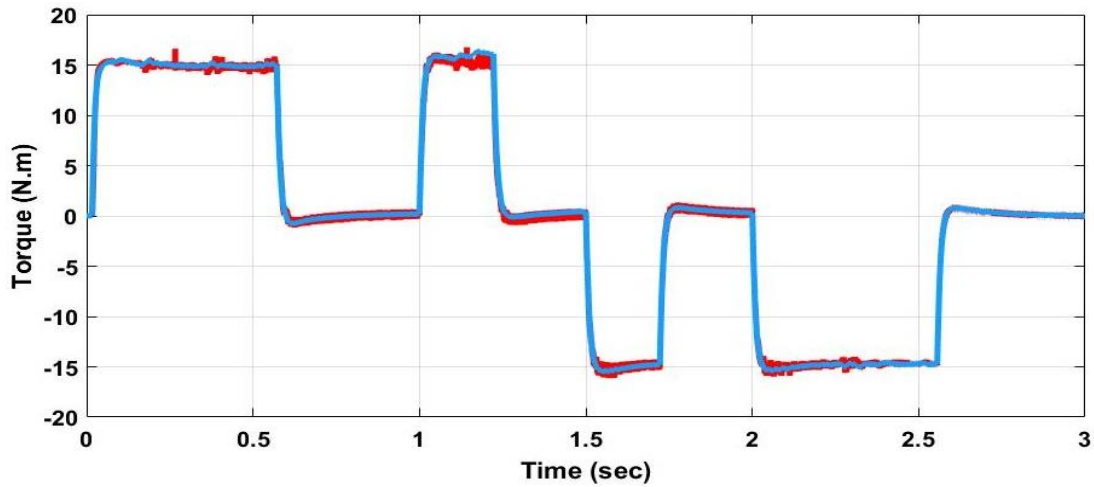


Fig. 12 Actual (red) and Reference Torque Dynamic (Blue).

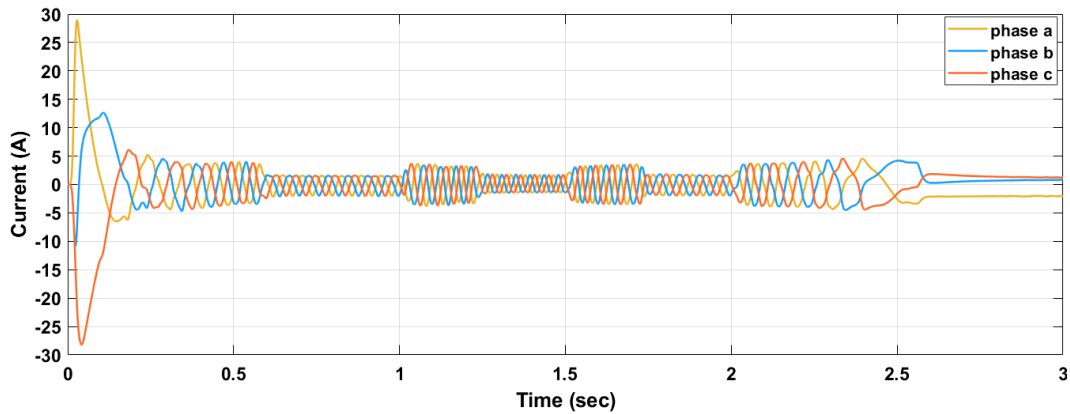


Fig. 13 Stator Current with the Proposed DTC Scheme Phase a, b, and c.

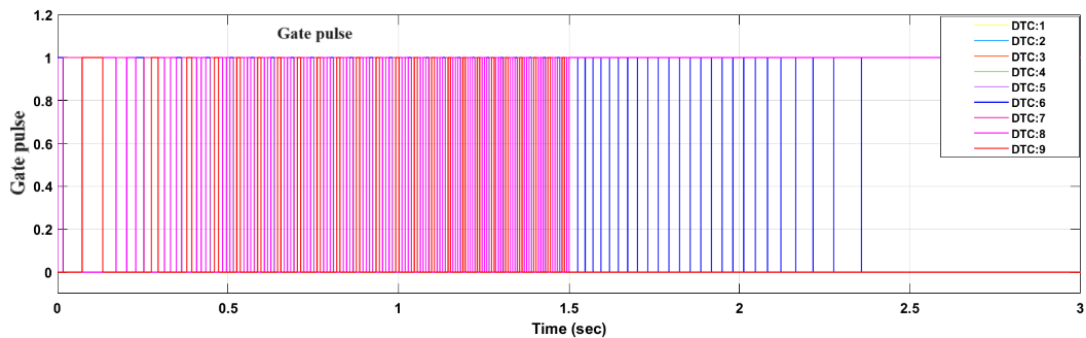


Fig. 14 Nine Gate Signals from (DTC1 to DTC9) to the Gate Drive the Matrix Converter.

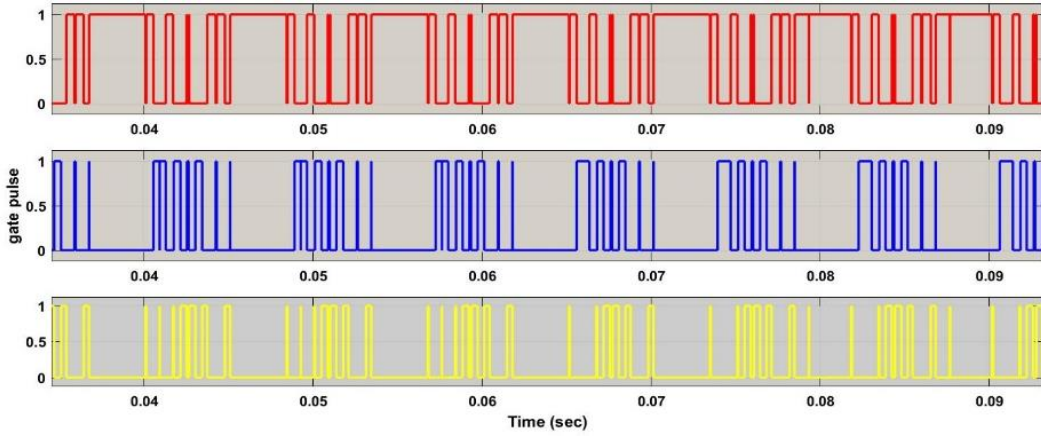


Fig. 15 Gate Signal of S11, S12, and S13 and Achieve Safe Switching Devices Commutation.

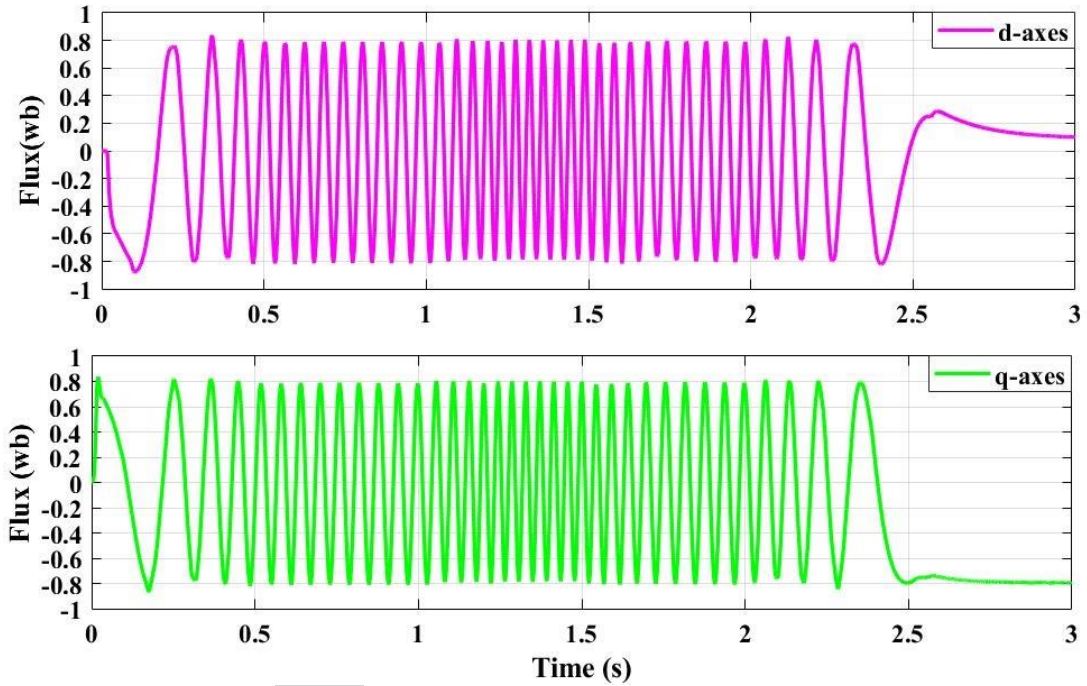


Fig. 16 Flux Stator for dq Axes Curve d-q axes.

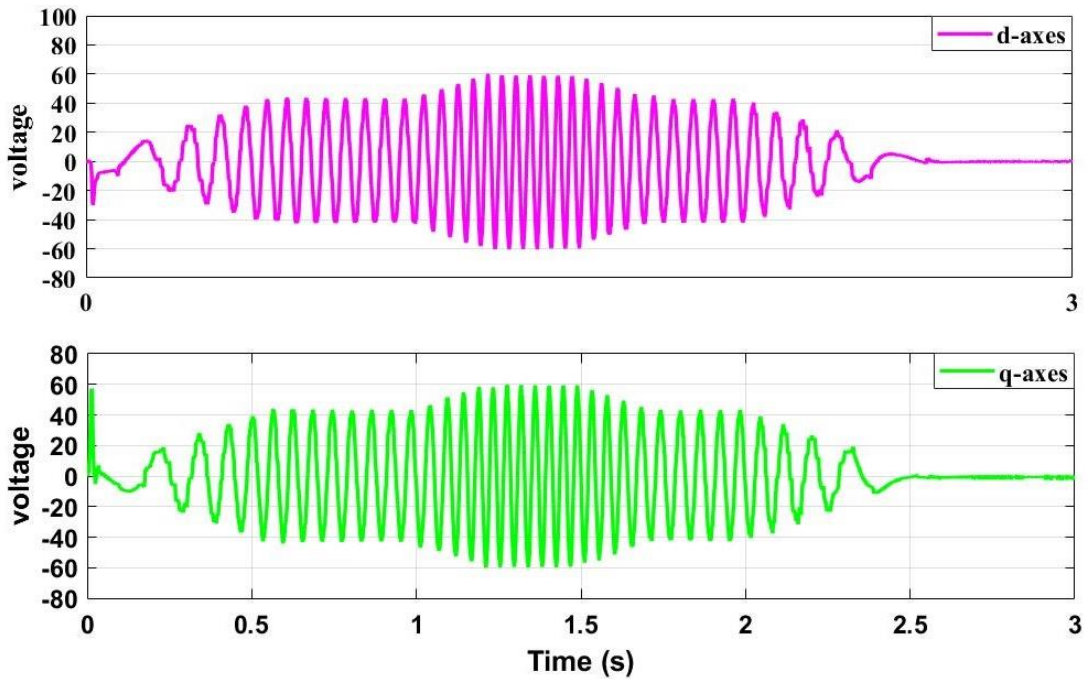


Fig. 17 Stator Voltage for dq Axes dq-Axes.

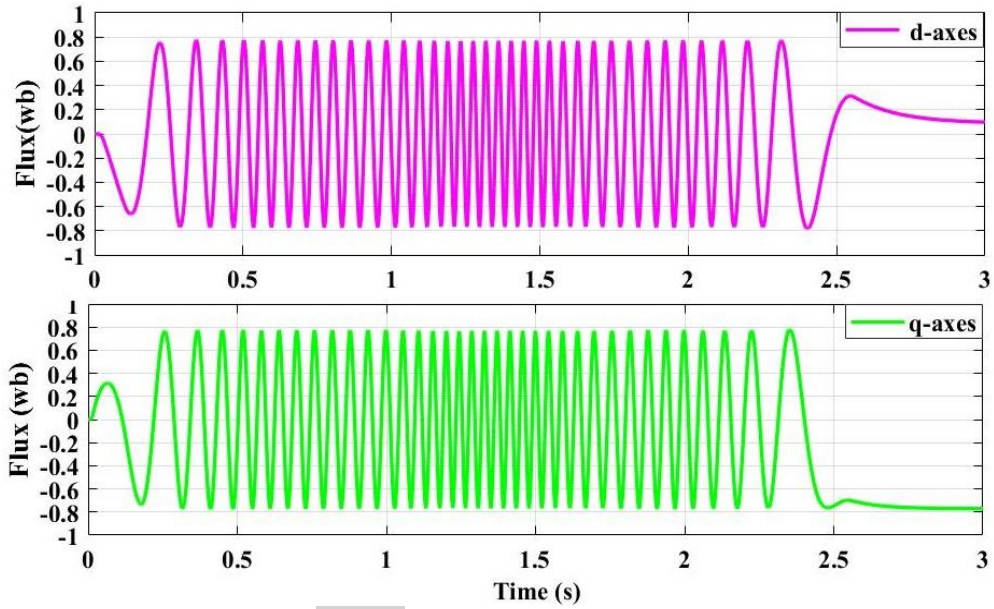


Fig. 18 Flux Rotor for dq Axes.

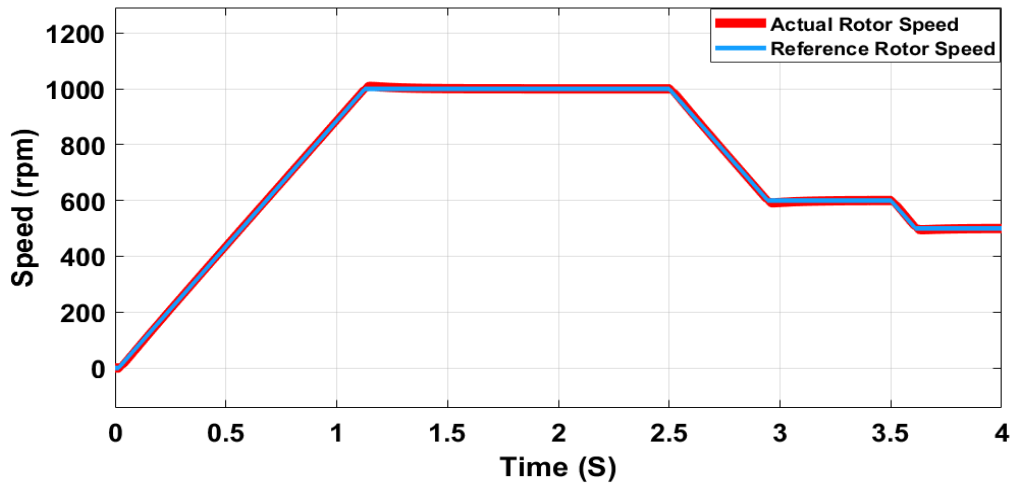


Fig. 19 Speed Reference in (blue) and Actual Speed Response in (red) at Speed References.

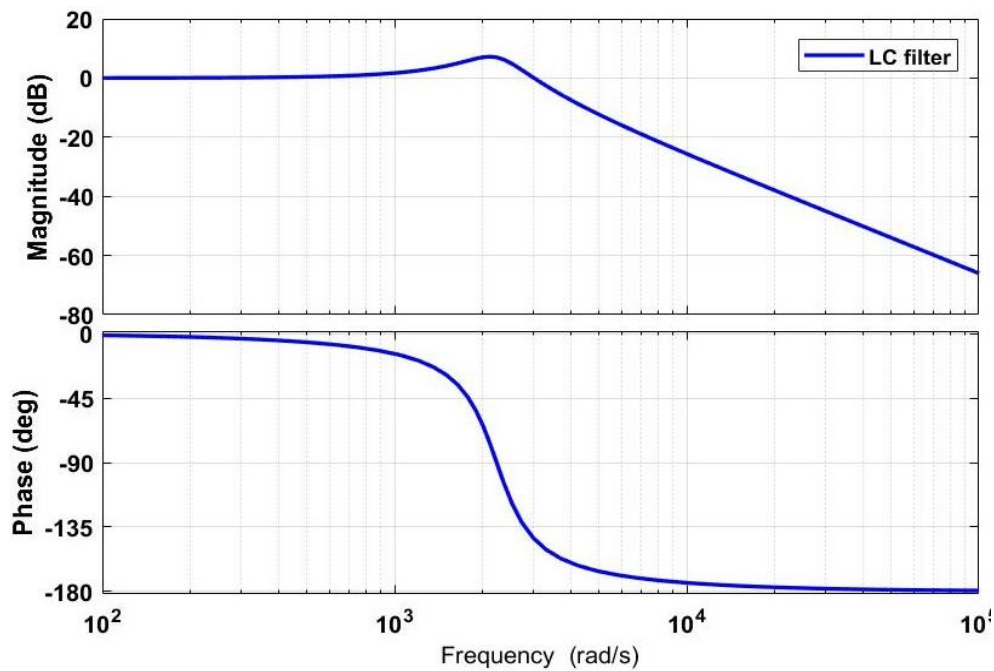


Fig. 20 LC-Filter Voltage Transfer Function.

7. CONCLUSION

The present study introduces the MC-DTC approach for induction motors, incorporating connecting DTC-MC with space vector modulation. This method seamlessly merges the benefits of DTC with SVM within the context of a matrix converter. A fresh switching table for DTC-SVM was proposed, offering comprehensive control over the induction motor requirements while maintaining the unity power factor at the input. Simulation results across a wide speed range validated the efficacy of this innovative control strategy. Moreover, the approach demonstrated improved input current harmonic characteristics and low-speed performance compared to the traditional MC-DTC approach. The approach also ensured the stability and reduction of flux, torque, and speed control. With its numerous advantages and promising prospects, further research is warranted.

REFERENCES

- [1] Rmili L, Ktata S, Yefrni K, Rahmani S, Al-Haddad K. **Overview of Matrix Converter: Topologies and Modulation.** *2022 IEEE 21st international Conference on Sciences and Techniques of Automatic Control and Computer Engineering (STA): IEEE;* 2022. pp. 465-470.
- [2] Son D-I, Han J-S, Park J-S, Lim H-S, Lee G-H. **Performance Improvement of DTC-SVM of PMSM with Compensation for the Dead Time Effect and Power Switch Loss Based on Extended Kalman Filter.** *Electronics* 2023;**12**(4):966, (1-17).
- [3] Sahri Y, Tamalouzt S, Lalouni Belaid S, Bacha S, Ullah N, Ahamdi AAA, Alzaed AN. **Advanced Fuzzy 12 DTC Control of Doubly Fed Induction Generator for Optimal Power Extraction in Wind Turbine System under Random Wind Conditions.** *Sustainability* 2021; **13**(21):11593, (1-23).
- [4] Sadat AR, Ahmadian S, Vosoughi N. **A Novel Torque Ripple Reduction of Switched Reluctance Motor Based on DTC-SVM Method.** *2018 IEEE Texas Power and Energy Conference (TPEC): IEEE;* 2018. pp. 1-6.
- [5] Muduli UR, Behera RK, Al Hosani K, El Moursi MS. **Direct Torque Control with Constant Switching Frequency for Three-to-Five Phase Direct Matrix Converter Fed Five-Phase Induction Motor Drive.** *IEEE Transactions on Power Electronics* 2022; **37**(9):11019-11033.
- [6] RK N. **Direct Torque Control for Matrix Converter Fed Induction Motor Using Svpwm.** *Proceedings of International Conference on Energy Efficient Technologies for Sustainability, St Xavier's Catholic College of Engineering, TamilNadu, India 5th to 7th April;* 2018.
- [7] Badiiee-Azandehi, A. Yousefi-Talouki, and M. Rezanejad. **Direct Torque Control Space Vector Modulation of Five-Phase Interior Permanent Magnet Synchronous Motor Using Matrix Converter.** *Australian Journal of Electrical and Electronics Engineering* 2015;**12**(2): 113-124.
- [8] De Klerk, Matthew Liam, Akshay Kumar Saha. **Performance Analysis of DTC-SVM in a Complete Traction Motor Control Mechanism for a Battery Electric Vehicle.** *Heliyon* 2022; **4**(6): 10-12.
- [9] Malla M, Gudey SK, Sudha S. **Transient and Steady State Characteristics of Induction Motor Drive Using Dtc-Svm Technique for Ev Applications.** *2020 11th International Conference on Electrical and Computer Engineering (ICECE): IEEE;* p. 403-406.
- [10] Hu Y, Huang S, Wu X, Li X. **Control of Dual Three-Phase Permanent Magnet Synchronous Machine Based on Five-Leg Inverter.** *IEEE Transactions on Power Electronics* 2019; **34**(11):11071-11079.
- [11] Kivanc O, Ozturk S. **Sector Determination for SVPWM Based Four-Switch Three-Phase VSI.** *Electronics Letters* 2017; **53**(5):343-345.
- [12] Thakre MP, Borse PS. **Analytical Evaluation of FOC and DTC Induction Motor Drives in Three Levels and Five Levels Diode Clamped Inverter.** *2020 International Conference on Power, Energy, Control and Transmission Systems (ICPECTS): IEEE;* 2020. pp. 1-6.
- [13] Zhang Z, Liu X. **A Duty Ratio Control Strategy to Reduce Both Torque and Flux Ripples of DTC for Permanent Magnet Synchronous Machines.** *IEEE Access* 2019; **7**:11820-11828.
- [14] Jassim AH, Hussein AA, Abbas LF. **The Performance of a Three-Phase Induction Motor under and over Unbalance Voltage.** *Tikrit Journal of Engineering Sciences* 2021; **28**(2): 15- 32.
- [15] RK N. **Direct Torque Control for Matrix Converter Fed Induction Motor Using SVPWM.** *Proceedings of International Conference on Energy Efficient Technologies for Sustainability, St Xavier's Catholic College of Engineering, TamilNadu, India 5th to 7th April;* 2018.
- [16] Zapar WM, Gaeid KS, Mokhlis H, Al-Smadi TA. **Review of the Most Recent**

- Articles in Fault Tolerant Control of Power Plants 2018 – 2022.** *Tikrit Journal of Engineering Sciences* 2023; **30**(2): 103- 113.
- [17] Hannan MA, Abd Ali J, Ker PJ, Mohamed A, Lipu MS, Hussain A. **Switching Techniques and Intelligent Controllers for Induction Motor Drive: Issues and Recommendations.** *IEEE Access* 2018; **6**:47489-47510.
- [18] Mansouri A, El Magri A, El Myasse I, Lajouad R, Elaadouli N. **Backstepping Nonlinear Control of a Five-Phase Pmsg Aerogenerator Linked to a Vienna Rectifier.** *Indonesian Journal of Electrical Engineering and Computer Science* 2023; **32**(2):734-741.
- [19] Gaeid KS, Al Smadi T, Abubakar U. **Double Control Strategy of Pmsm Rotor Speed-Based Traction Drive Using Resolver.** *Results in Control and Optimization* 2023; **13**:100301, (1-12).
- [20] Mansouri A, El Magri A, Lajouad R, Giri F. **Control Design and Multimode Power Management of Wecs Connected to Hvdc Transmission Line through a Vienna Rectifier.** *International Journal of Electrical Power & Energy Systems* 2024; **155**:109563, (1-13).
- [21] Velerander E, Kruse L, Wiik T, Wiberg A, Colmenares J, Nee HP. **An IGBT Turn-on Concept Offering Low Losses under Motor Drive Dv/Dt Constraints Based on Diode Current Adaption.** *IEEE Transactions on Power Electronics* 2017; **33**(2):1143-1153.
- [22] Varajao D, Araújo RE. **Modulation Methods for Direct and Indirect Matrix Converters: A Review.** *Electronics* 2021; **10**(7):812, (1-29).
- [23] Liu Z, Li Y, Zheng Z. **A Review of Drive Techniques for Multiphase Machines.** *CES Transactions on Electrical Machines and Systems* 2018; **2**(2):243-251.
- [24] Dash L, Pattanayak BK, Laha SR, Pattnaik S, Mohanty B, Habboush AK, Al Smadi T. **Energy Efficient Localization Technique Using Multilateration for Reduction of Spatially and Temporally Correlated Data in RFID System.** *Tikrit Journal of Engineering Sciences* 2024; **31**(1): 101-112.
- [25] Ramasamy P, Vakesan K, Govindaraj V, Venkatarajan S, Chattopadhyay S, Sugavanam V. **A Novel Svpwm for 3-Phase to 5-Phase Conversion Using Matrix Converter.** *International Journal of Power Electronics and Drive Systems* 2022; **13**(4): 2269-2276.
- [26] Siami M, Khaburi DA, Rodriguez J. **Simplified Finite Control Set-Model Predictive Control for Matrix Converter-Fed PMSM Drives.** *IEEE Transactions on Power Electronics* 2017;**33**(3):2438-2446.
- [27] Al Smadi T, Handam A, Gaeid KS, Al-Smadi A, Al-Husban Y. **Artificial Intelligent Control of Energy Management PV System.** *Results in Control and Optimization* 2024; **14**: 100343, (1-13).
- [28] Abbas LF, Ahmed REA, Mahmmoud ON, Gaeid KS, Mokhlis HB. **Single Phasing Effects on the Behavior of Three phase Induction Motor.** *Tikrit Journal of Engineering Sciences* 2023; **30**(4):11-18.
- [29] Gaeid KS, Murshid AM, Salih ZH. **Direct Torque Control of Induction Motor with Matrix Converter.** *Journal of Engineering Science & Technology Review* 2016; **9**(2): 50-58.
- [30] Siwek P. **Input Filter Optimisation for a DTC Driven Matrix Converter-Fed PMSM Drive.** *2018 23rd International Conference on Methods & Models in Automation & Robotics (MMAR)*: IEEE; 2018. pp. 35-40.
- [31] Atangana A, Akgül A. **Can Transfer Function and Bode Diagram Be Obtained from Sumudu Transform.** *Alexandria Engineering Journal* 2020;**59**(4):1971-1984.